PHILOSOPHICAL TRANSACTIONS A

royalsocietypublishing.org/journal/rsta

Research

Cite this article: Jiao W, Shu H, He Q, Raney JR. 2024 Toward mechanical proprioception in autonomously reconfigurable kirigami-inspired mechanical systems. *Phil. Trans. R. Soc. A* **382**: 20240116.
https://doi.org/10.1098/rsta.2024.0116

Received: 29 February 2024
Accepted: 8 August 2024

One contribution of 16 to a theme issue 'Origami/Kirigami-inspired structures: from fundamentals to applications'.

Subject Areas:
mechanical engineering

Keywords:
mechanical proprioception, reconfigurable materials, multistable kirigami

Author for correspondence:
Jordan R. Raney
e-mail: raney@seas.upenn.edu

Electronic supplementary material is available online at https://doi.org/10.6084/m9.figshare.c.7461942.

THE ROYAL SOCIETY PUBLISHING

Toward mechanical proprioception in autonomously reconfigurable kirigami-inspired mechanical systems

Weijian Jiao[1,2,3], Hang Shu[1], Qiguang He[1,4] and Jordan R. Raney[1]

[1]Department of Mechanical Engineering and Applied Mechanics, University of Pennsylvania, Philadelphia, PA 19104, USA
[2]School of Aerospace Engineering and Applied Mechanics, Tongji University, Shanghai 200092, People's Republic of China
[3]Shanghai Institute of Aircraft Mechanics and Control, Shanghai 200092, People's Republic of China
[4]Department of Mechanical and Automation Engineering, The Chinese University of Hong Kong 999077, Hong Kong

JRR, 0000-0001-5329-9980

Mechanical metamaterials have recently been exploited as an interesting platform for information storing, retrieval and processing, analogous to electronic devices. In this work, we describe the design and fabrication a two-dimensional (2D) multistable metamaterial consisting of building blocks that can be switched between two distinct stable phases, and which are capable of storing binary information analogous to digital bits. By changing the spatial distribution of the phases, we can achieve a variety of different configurations and tunable mechanical properties (both static and dynamic). Moreover, we demonstrate the ability to determine the phase distribution via simple probing of the dynamic properties, to which we refer as mechanical proprioception. Finally, as a simple demonstration of feasibility, we illustrate a strategy for building autonomous kirigami systems that can receive inputs from their environment. This work could bring new insights for the design of mechanical metamaterials with information processing and computing functionalities.

This article is part of the theme issue 'Origami/Kirigami-inspired structures: from fundamentals to applications'.

1. Introduction

Mechanical metamaterials have drawn significant interest in recent years because they allow facile control of a wide range of mechanical properties [1–3], including static properties, such as the Poisson's ratio (including negative Poisson's ratio), and dynamic properties, such as band gaps. Despite these intriguing properties, most mechanical metamaterials have a fixed set of mechanical properties, meaning that a new system must be designed and fabricated if different properties are desired. However, a subset of mechanical metamaterials are reconfigurable, allowing state changes to occur after fabrication, leading to a range of tunable properties [4–10]. Origami- and kirigami-inspired mechanical metamaterials are chief among these. First, they allow a large range of mechanical properties to be selected based on a few simple fold and cut patterns [11–15], including enhanced stiffness [13], negative Poisson's ratio [15] and multistability [12,16,17]. These principles have been adopted in various engineering applications such as robotics [18] and reconfigurable structures [19]. Second, the internal creases and/or cuts often allow reconfiguration of shape and mechanical properties via simple static loads [19].

Beyond the common properties of interest mentioned above, such as control of stiffness, Poisson's ratio and band gaps, recent research has begun to explore whether such mechanical metamaterials can be used to control more exotic properties, including the processing of information itself (i.e. mechanical computing) [20,21]. That is, just as traditional mechanical properties such as stiffness, strength and linear wave propagation can be varied in mechanical metamaterials via the control of relevant design parameters such as cut patterns, nodal mass, hinge thickness, etc., can the static configuration or dynamic properties of such systems be used to process, and sometimes store, information [22–24]? In some cases, binary mechanical digits can be represented by bistable mechanisms, which can be achieved in practice in beam-based [23,25–28], origami [29] and kirigami [30] designs, among others. These mechanisms support two (or sometimes more) equilibrium states, which can be abstracted as information states that one may label as '0', '1', etc. Because bistable mechanisms maintain their state even after a mechanical load is removed from the system, such mechanical bits can also be thought of as stable memory [31] to store information. In other cases, such mechanical metamaterials are designed to perform information processing tasks such as counting mechanical driving cycles [32], forming a network of logic gates [33] and sequential encoding of information through external stimuli [34].

While there have been many demonstrations, as above, of the design of mechanical metamaterials, including origami and kirigami designs, that can process information, it is still unclear how such systems should be interfaced with their environment, and how one should read the 'output' of a computational event. Unlike conventional digital electronics, when a mechanical system computes, it is often associated with a change in shape and, often, mechanical properties. Utilizing the deformation of kirigami structures in response to external stimuli, e.g. forces, researchers have developed strain [35], pressure [36] and multimodal sensors incorporated with electronic components to achieve sensing and monitoring capabilities [37,38].

Here, we build on the above work from the research community to numerically and experimentally consider the design of a kirigami-based multistable metamaterial that is capable of autonomously performing simple information state changes based on the environment. These state changes are associated with changes in state of bistable building blocks that can autonomously switch between two distinct stable phases. To achieve this, we incorporate stimuli-responsive materials with the local bistable units, allowing them to sense the local

environment and, if defined conditions are met, to change state in response. Moreover, we consider a strategy for 'reading out' the information state of the system: as the local bistable states change, the global structure itself changes, which is associated with changes in mechanical properties such as stiffness and linear wave propagation. Hence, there is potential to determine the phase distribution via simple probing of the mechanical properties (e.g., the dynamic response), which we refer to as mechanical proprioception. This could allow one to read the encoded information even if the metamaterial is operated in an environment where visual observation or optical characterization is not feasible.

First, we describe the design of the multistable kirigami, which is based on the rotating-squares mechanism [39–42]. Here, the building block consists of 4×4 squares connected by thin hinges (see schematic in figure 1*a*). Permanent magnets are inserted into each square with alternating polarization. If the squares are subjected to rotation with respect to one another, the competition between the strain energy of the hinge and the interaction of the magnets can lead to three stable angles (phases) of the building block: one open phase and two closed phases. The closed phases have identical mechanical properties but are obtained via opposite rotations of the squares. For simplicity, we only consider one of the closed phases in this study. Multiple building blocks can be joined together to form a larger two-dimensional (2D) kirigami metamaterial. The metamaterial comprises 4×4 such building blocks connected with the pattern shown by the black bars in figure 1*a*. If instead the building blocks are joined together at all possible squares, the mechanical coupling is sufficiently high that the entire 2D metamaterial takes on the same phase (see, for example, [43]). The decreased mechanical coupling obtained by removing some of the connections between squares in adjacent building blocks allows each individual building block to have its own phase independent of neighbouring building blocks. As a result, different phase distributions can be realized in the mechanical metamaterial. For the experiments, we fabricated the specimens by three-dimensionally printing a mould (MakerGear M2, polylactic acid) and then cast a silicone precursor (Dragon Skin 10) into it. The specimens where then cured and extracted from the mould; a photograph of the metamaterial prototype is shown in figure 1*b*.

To quantify the effects of different design parameters, we rely on a discrete model established previously for similar systems [43,44]. Each square has side length L and is assumed to be a rigid body with mass M and moment of inertia J ($L = 12 \times 10^{-3}$ m, $M = 2.501 \times 10^{-3}$ kg and $J = 60.024 \times 10^{-9}$ kg·m2 for the metamaterial prototype). As shown in figure 1*c*, each square has two translational degrees of freedom (u and v) and one rotational degree of freedom (θ). Each hinge is modelled by three springs: a linear longitudinal spring with stiffness K_l, a linear shear spring with stiffness K_s and a nonlinear torsional spring with potential energy $E_\theta(\Delta\theta)$ expressed as (the explicit expressions for the potentials of the longitudinal and shear springs are given in electronic supplementary material, note 1)

$$E_\theta(\Delta\theta) = \frac{1}{2}K_\theta(\Delta\theta)^2 + V_{\text{Morse}}(\Delta\theta), \tag{1.1}$$

$$V_{\text{Morse}}(\Delta\theta) = A\left[e^{2\alpha(\Delta\theta - 2\theta_M)} - 2e^{\alpha(\Delta\theta - 2\theta_M)}\right] + A\left[e^{-2\alpha(\Delta\theta + 2\theta_M)} - 2e^{-\alpha(\Delta\theta + 2\theta_M)}\right], \tag{1.2}$$

where the first term on the right-hand side of equation (1.1) captures the linear bending behaviour of the hinge (K_θ is the linear torsional spring constant and $\Delta\theta$ is the relative angle of the hinge), and the second term, V_{Morse}, is the Morse potential, used to empirically describe the nonlinear magnetic interactions between squares. In equation (1.2), A and α define the depth and width of the Morse potential, respectively, and $\pm\theta_M$ determines its equilibrium angles. To obtain these parameters for the discrete model, we conducted a series of experimental tensile tests using a commercial quasistatic test system (Instron model 68SC-5) with custom fixtures that are designed to allow the squares to rotate during the tests (see electronic supplementary

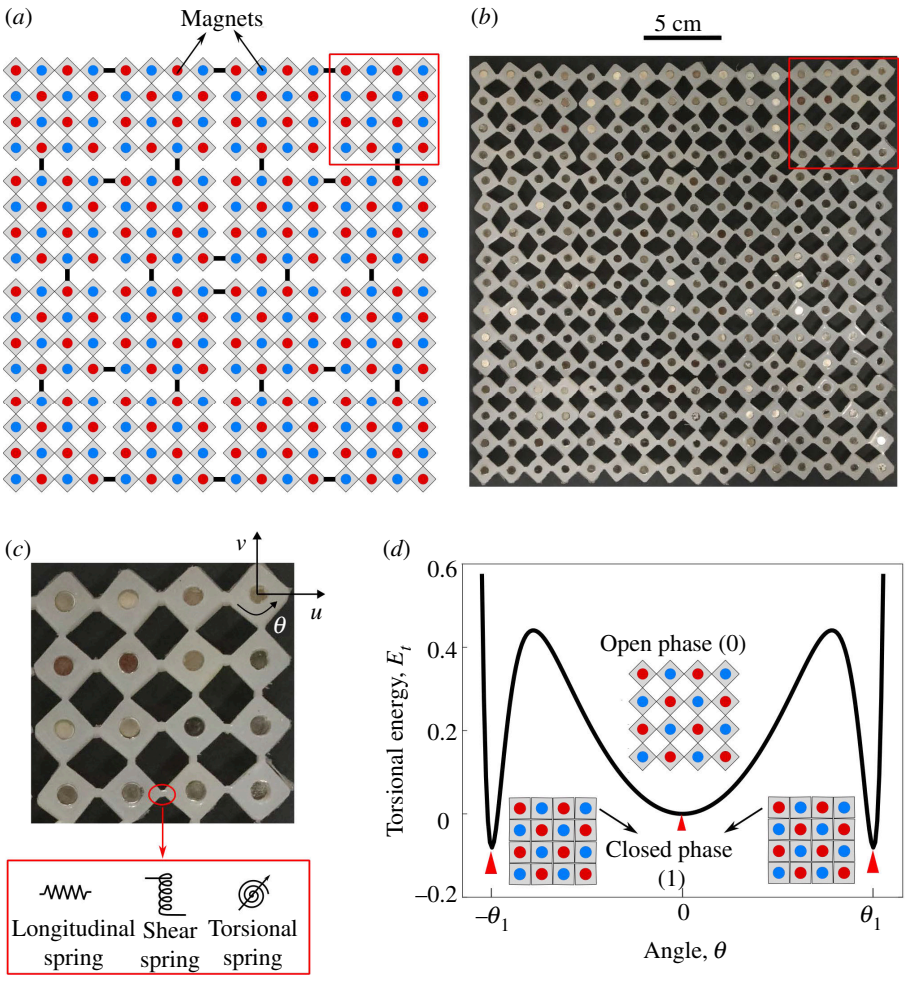

Figure 1. (*a*) Schematic of the multistable metamaterial. The red box indicates a building block consisting of 4 × 4 squares. (*b*) A photograph of the metamaterial prototype. (*c*) An experimental image of a building block (with magnets at the centres of the squares). A discrete model is developed for this system by treating the hinges as springs and accounting for multistability via an empirical torsional spring component.(*d*) Torsional energy landscape of the ligament, exhibiting an open phase (0) and two closed phases (1).

material, note 2, for details). Using the experimentally obtained parameters ($K_l \approx 3.958 \times 10^2$ N/m, $K_s \approx 58$ N/m, $K_\theta \approx 2.5 \times 10^{-4}$ N·m/rad, $A \approx 2 \times 10^{-4}$, $\alpha \approx 8.5$, $\theta_M \approx 45°$) we calculated the multistable energy landscape from equation (1.1), which exhibits three distinct phases at angles $\theta = 0, \pm\theta_1$, as shown in figure 1*d*. Note that θ_1 can be slightly different from θ_M as a result of the interaction between the linear torsional spring and the Morse potential.

Next, we experimentally and numerically demonstrate the reconfigurability of the metamaterial, which is achieved by changing the phases of the building blocks (i.e. phase distribution). As shown in figure 2, a variety of configurations are experimentally achieved by forcing certain blocks from the initial open phase into the closed phase, ranging from two blocks closed at the top centre (figure 2*a*) to all-closed blocks (figure 2*f*). The numerical results obtained from full-scale simulations agree well with the experimental demonstrations. Specifically, we performed the full-scale simulations by numerically solving the equations of motion (EoMs) of the system using the fourth-order Runge–Kutta method (see electronic supplementary material, note 1, for the derivation of the EoMs and the detailed set-up of the numerical simulations). A phase transformation from the open to a closed phase is associated with a large decrease in

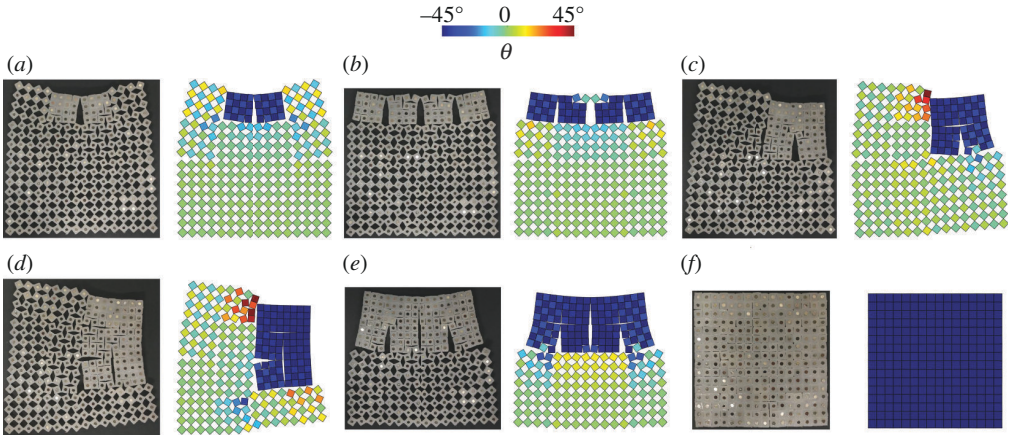

Figure 2. Reconfigurability of the multistable metamaterial (photographs are from experiments, and coloured images are from numerical simulations). (*a*) A configuration with two blocks closed at the top centre. (*b*) A configuration with 1×4 blocks closed at the top. (*c*) A configuration with 2×2 blocks closed at the top-right corner. (*d*) A configuration with 3×2 blocks closed at the top-right corner. (*e*) A configuration with 2×4 blocks closed at the top. (*f*) All-closed configuration.

area. This induces internal forces that render certain phase distributions unachievable (e.g. a closed block in the interior surrounded by all open blocks). Interestingly, under impact loading the metamaterial can transform into some simple configurations (e.g. two blocks closed at the exterior) via nonlinear dynamics, which were captured by a high-speed camera (Photron FASTCAM Mini AX; see Movie).

We now focus on the mechanical properties of the multistable kirigami, and especially on how these properties can be tuned by reconfiguring the structure with different phase distributions. First, we experimentally investigated the static properties of four different configurations of the metamaterial sample, as reported in electronic supplementary material, note 3. Then, we used the discrete model to numerically investigate how the dynamic properties can be influenced by the spatial distribution of different phases. It is expected that different phases can exhibit distinct dynamic behaviours, and, therefore, that different phase distributions may result in distinct global dynamic behaviours of the system. This enabled us to do the reverse: to determine the phase distribution via simple probing of the dynamic properties. Here, we considered a metamaterial following the same design but with a different set of parameters: $M = 2 \times 10^{-3}$ kg, $J = 46.6 \times 10^{-9}$ kg·m^2, $L = 20 \times 10^{-3}$ m, $K_l = 287.2$ N/m, $K_s = 68.8$ N/m, $K_\theta = 1.7 \times 10^{-4}$ N·m/rad, $A = 2.1 \times 10^{-4}$, $\alpha = 5.5$, $\theta_M = 44°$. We deliberately chose the above parameters to obtain the desired dispersion relations, which exhibit distinct dispersive characteristics for open and closed phases (see electronic supplementary material, note 4, for the complete band diagrams obtained via unit cell analysis). For illustrative purposes, we consider the following configurations of the metamaterial and their possible variants: the all-open configuration, the all-closed configuration, a configuration with 2×2 blocks closed at one corner and a configuration with 2×4 blocks closed at one edge. The configurations considered here are shown in electronic supplementary material, figure S6.

Next, we performed a steady-state vibration analysis for each configuration. Specifically, a harmonic moment $M = M_0 e^{i2\pi ft}$ (M_0 denotes the amplitude of the moment and f denotes the excitation frequency) was prescribed as an input to the square at the left-bottom corner, and the rotational responses $\Theta_p(f)$, $p = 1,2,3$ were measured from the squares at the other three corners, i.e. the three outputs indicated in figure 3. As detailed in electronic supplementary material, note 5, a steady-state response $\mathbf{U}(f)$ (note that $\Theta_p(f)$ are the components of $\mathbf{U}(f)$ that correspond to the rotational degrees of freedom of the three outputs) is obtained by solving the following equation:

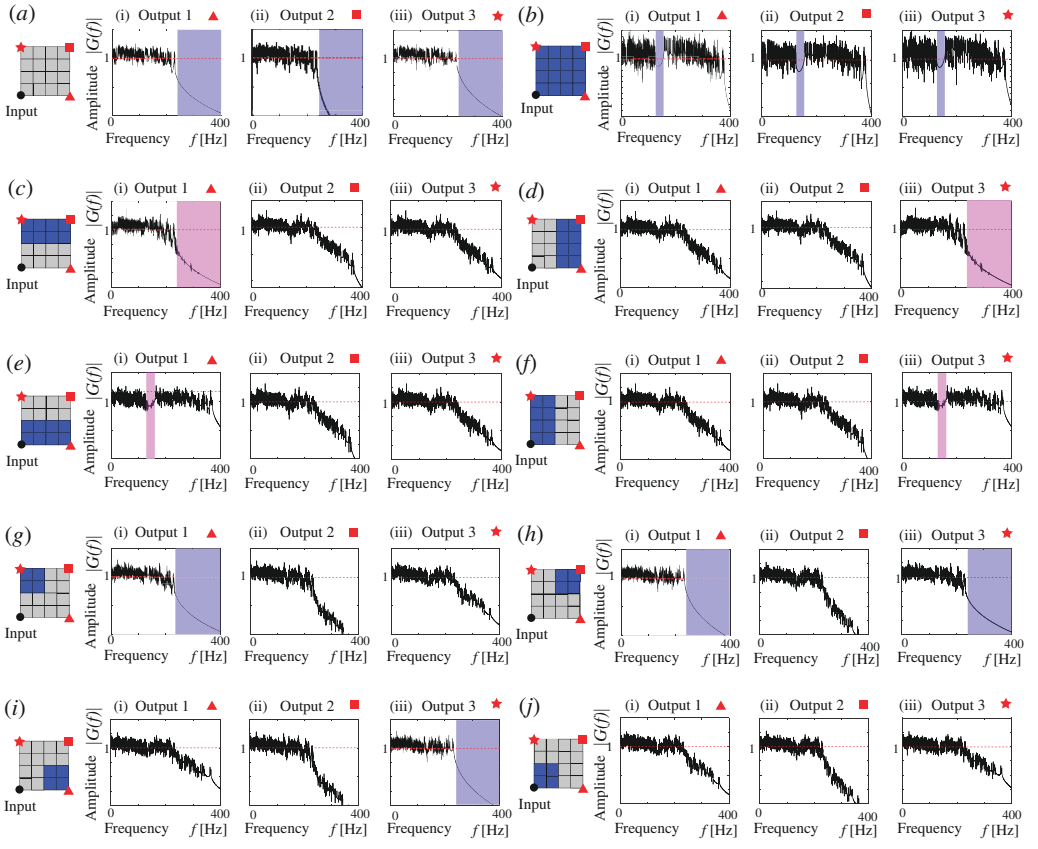

Figure 3. Mechanical proprioception: determining spatial phase distribution via probing dynamic properties of the metamaterial. For an input fixed at the bottom-left corner, magnitude of the frequency response is obtained at the rest three corners (i.e. fixed output 1, 2, 3) for (*a*) all-open configuration, (*b*) all-closed configuration, (*c–f*) four possible variants of a configuration with 2×4 building blocks closed, (*g–j*) four possible variants of a configuration with 2×2 building blocks closed. Frequency ranges highlighted in purple (or pink) indicate the existence of clean (or slightly blemished) band gaps. It can be observed that the three outputs of one variant exhibit dynamic properties that are noticeably different from any other variants, a step toward mechanical proprioception.

$$\left[-\omega^2\mathbf{M} + \mathbf{K}(\bar{\mathbf{u}})\right]\mathbf{U}(f) = \mathbf{F}_0, \tag{1.3}$$

where $\mathbf{M}$, $\mathbf{K}$, $\mathbf{F}_0$ and $\bar{\mathbf{u}}$ are the mass matrix, stiffness matrix, external force/moment amplitude vector and current displacement vector, respectively. Moreover, the stiffness matrix $\mathbf{K}(\bar{\mathbf{u}})$ depends on the current displacement vector $\bar{\mathbf{u}}$. It is obvious that different configurations are associated with different $\bar{\mathbf{u}}$ and $\mathbf{K}(\bar{\mathbf{u}})$. Therefore, in principle, different phase distributions would exhibit distinct steady-state responses.

In figure 3, we report the magnitude of the frequency response $|G(f)| = |\Theta_p(f)/M_0|$ as a function of the excitation frequency f for all possible phase distributions. When $|G(f)| < 1$ for a frequency range, we may identify the existence of a cut-off frequency or a bandgap (a clean one is highlighted in purple, while a less clean one is highlighted in pink). From the outputs given in figure 3*a*,*b*, we find that the all-open configuration has a much lower cut-off frequency than that of the all-closed configuration. Also, the all-closed configuration has a very narrow band gap near $f = 140$ Hz. Interestingly, the three outputs are different from one phase distribution to another, which gives rise to a unique correspondence between the dynamic behaviour and the phase distribution. This correspondence allows the reverse task, i.e., determining the phase distribution via probing its dynamic properties, which we term mechanical proprioception. As

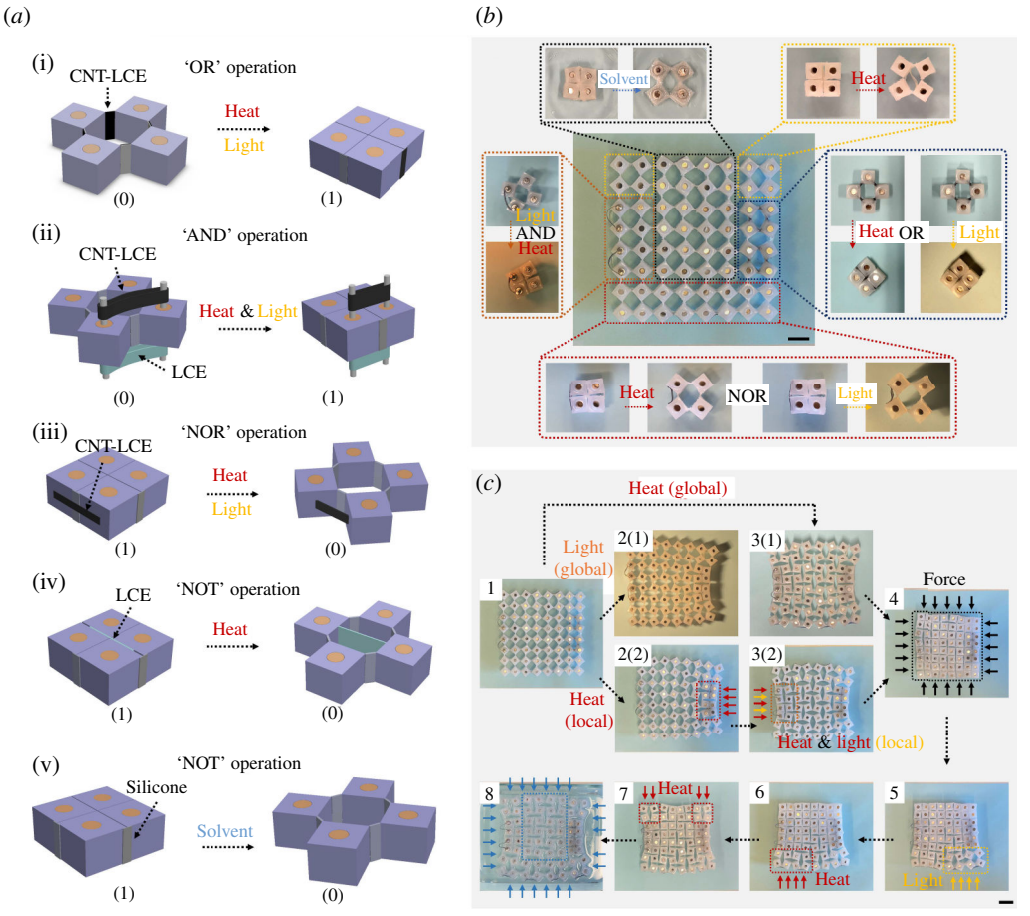

Figure 4. Autonomous phase transformations in a 2D multistable kirigami metamaterial with stimuli-responsive materials. (*a*) Schematics showing the integration of stimuli-responsive materials and associated mechanisms with the rotating squares, enabling transformation between open and closed states in response to different environments (heat, light, and solvents). (*b*) Experimental images of an 8 × 8 multistable kirigami structure with the mechanisms of (*a*) incorporated into different regions of the structure.(*c*) Experimental images of the kirigami in different configurations; the labels and arrows indicate how introduction of different stimuli affect the structure. Scale bars in (*b*) and (*c*): 1 cm.

expected, this concept can, in principle, be used to determine arbitrary phase distributions. For example, we performed a steady-state analysis for a more complex phase distribution involving two different closed states for which the frequency responses were different from those presented in figure 3, as reported in electronic supplementary material, figure S7.

In addition to the above relationships, which could potentially allow one to read the 'output' of a computational event via measurements of the metamaterial's mechanical properties (rather than viewing it optically to explicitly characterize the distribution of phases, for example), we conclude by considering how the mechanical system might also autonomously receive inputs from the environment. Here, as a simple demonstration of feasibility, our basic strategy for achieving this is to incorporate responsive materials, such as liquid crystal elastomers (LCEs) and silicones, into the kirigami-inspired metamaterial. These materials locally deform in response to temperature and non-polar solvents, effectively acting as sensors for these environmental parameters. Figure 4*a* shows several examples of mechanisms by which these materials can be incorporated into the kirigami pattern and thereby translate the material-specific response to a particular stimulus into a structural change of the kirigami. Schematic (i) shows a mechanism that acts like an 'OR' operation, where exposure to either heat or light will move the local state of the kirigami from open (0) to closed (1). The mechanism illustrated in

(ii) is similar, but acts as an 'AND' operation for this stimuli (i.e. requiring both stimuli to be present to close the kirigami). Schematics (iii–v) show mechanisms that will move the local state from closed (1) to open (0). Additional information can be found in electronic supplementary material, figures S8 and S9, describing the state change with respect to time.

In these examples, the integrated responsive materials include LCEs, carbon nanotube (CNT)-doped LCEs and PDMS-glass fibre composites, which actuate in response to heat, light/heat, and non-polar solvents, respectively. For example, LCEs undergo a nematic to isotropic phase transition if the temperature is increased above a threshold, causing anisotropic contraction [45]. If the CNTs are included in the LCEs, a photothermal effect is enabled [46], with the CNTs absorbing light and locally raising the temperature, allowing the composite to actuate in response to heat or light. The PDMS-glass fibre composite swells anisotropically in the presence of non-polar solvents, such as hexane and toluene [27].

The type and placement of responsive materials, together with the type of mechanism (e.g. figure 4*a*), determine the local and global changes in the kirigami metamaterials that occur in the presence of different stimuli [47]. As an example, figure 4*b* shows experimental images of an 8×8 structure and indicates the locations of the different mechanisms in the structure (and their associated effects). Based on this arrangement of mechanisms, figure 4*c* provides experimental images showing how this structure autonomously rearranges when different stimuli are applied. Here, 'global' indicates that the associated stimulus is applied to the entire specimen, while 'local' means that the associated stimulus is only applied where indicated. 'Force' indicates that the phase distribution in the structure is manually changed via a mechanical force. For example, if we apply heat globally, the kirigami changes shape from configuration 1 to 3, with units on the left- and right-hand side closed. As another example, the bottom part of the structure transitions from closed (1) to open (0) if heat or light is applied. Additional configuration changes are indicated in figure 4*c*. Finally, as described earlier (e.g. figure 3), different configurations (phase distributions) can be associated with different mechanical properties. In principle, the combined strategy of (i) incorporating stimuli-responsive materials with kirigami to act as sensors and (ii) mapping configuration changes to changes in mechanical properties could enable the development of intelligent kirigami metamaterials that can perform simple operations autonomously, serving as a demonstration of mechanical logic.

In summary, we have designed a 2D reconfigurable, multistable kirigami metamaterial that can encode binary information via the spatial distribution of its phases. The mechanical properties of the system vary according to this spatial distribution. Since the mechanical properties thereby correspond to the information state of the system, the information state can, in principle, be read out by simply probing the static and dynamic properties, which we term mechanical proprioception. This concept, along with the proposed strategy for incorporating stimuli-responsive materials, could be utilized in applications in information processing, mechanical computing and physical intelligence.

Data accessibility. Supplementary material is available online [48].

Declaration of AI use. We have not used AI-assisted technologies in creating this article.

Authors' contributions. W.J.: conceptualization, data curation, formal analysis, investigation, methodology, validation, visualization, writing—original draft, writing—review and editing; H.S.: data curation, formal analysis, investigation, methodology, visualization, writing—original draft, writing—review and editing; Q.H.: conceptualization, data curation, investigation, methodology, visualization, writing—original draft, writing—review and editing; J.R.R.: conceptualization, formal analysis, funding acquisition, investigation, project administration, resources, supervision, writing—original draft, writing—review and editing.

All authors gave final approval for publication and agreed to be held accountable for the work performed therein.

Conflict of interest declaration. We declare we have no competing interests.

Funding. The authors gratefully acknowledge support for this work provided by DARPA Young Faculty Award grant number W911NF2010278, AFOSR award number FA9550-23-1-0416 and National Science Foundation award numbers 2041410 and 2239308. W.J. acknowledges support from the Fundamental

Research Funds for the Central Universities (grant number 22120240045) and Shanghai Gaofeng Project for University Academic Program Development.

References

1. Babaee S, Shim J, Weaver JC, Chen ER, Patel N, Bertoldi K. 2013 3D soft metamaterials with negative poisson's ratio. *Adv. Mater.* **25**, 5044–5049. (doi:10.1002/adma.201301986)
2. Liu Z, Zhang X, Mao Y, Zhu Y, Yang Z, Chan CT, Sheng P. 2000 Locally resonant sonic materials. *Science* **289**, 1734–1736. (doi:10.1126/science.289.5485.1734)
3. Zhang K, Jiao W, Gonella S. 2021 Tunable band gaps and symmetry breaking in magnetomechanical metastructures inspired by multilayer two-dimensional materials. *Phys. Rev. B* **104**, L020301. (doi:10.1103/PhysRevB.104.L020301)
4. Florijn B, Coulais C, van Hecke M. 2014 Programmable mechanical metamaterials. *Phys. Rev. Lett.* **113**, 175503. (doi:10.1103/PhysRevLett.113.175503)
5. Jesse L, Evans AA, McLeod L, Hayward RC, Hull T, Santangelo CD, Cohen I. 2014 Applied origami. using origami design principles to fold reprogrammable mechanical metamaterials. *Science* **345**, 647–650. (doi:10.1126/science.1252876)
6. Schaeffer M, Ruzzene M. 2015 Wave propagation in reconfigurable magneto-elastic kagome lattice structures. *J. Appl. Phys.* **117**, 194903. (doi:10.1063/1.4921358)
7. Celli P, Gonella S. 2015 Manipulating waves with LEGO® bricks: a versatile experimental platform for metamaterial architectures. *Appl. Phys. Lett.* **107**, 8. (doi:10.1063/1.4929566)
8. Yang D, Jin L, Martinez RV, Bertoldi K, Whitesides GM, Suo Z. 2016 Phase-transforming and switchable metamaterials. *Extreme Mech. Lett.* **6**, 1–9. (doi:10.1016/j.eml.2015.11.004)
9. Fang X, Wen J, Cheng L, Yu D, Zhang H, Gumbsch P. 2022 Programmable gear-based mechanical metamaterials. *Nat. Mater.* **21**, 869–876. (doi:10.1038/s41563-022-01269-3)
10. Xiu H, Liu H, Poli A, Wan G, Sun K, Arruda EM, Mao X, Chen Z. 2022 Topological transformability and reprogrammability of multistable mechanical metamaterials. *Proc. Natl Acad. Sci.* **119**, e2211725119. (doi:10.1073/pnas.2211725119)
11. Zhu R, Yasuda H, Huang GL, Yang JK. 2018 Kirigami-based elastic metamaterials with anisotropic mass density for subwavelength flexural wave control. *Sci. Rep.* **8**, 483. (doi:10.1038/s41598-017-18864-z)
12. Yasuda H, Tachi T, Lee M, Yang J. 2017 Origami-based tunable truss structures for non-volatile mechanical memory operation. *Nat. Commun.* **8**, 1–7. (doi:10.1038/s41467-017-00670-w)
13. Filipov ET, Tachi T, Paulino GH. 2015 Origami tubes assembled into stiff, yet reconfigurable structures and metamaterials. *Proc. Natl Acad. Sci.* **112**, 12321–12326. (doi:10.1073/pnas.1509465112)
14. Lv C, Krishnaraju D, Konjevod G, Yu H, Jiang H. 2014 Origami based mechanical metamaterials. *Sci. Rep.* **4**, 5979. (doi:10.1038/srep05979)
15. Yasuda H, Yang J. 2015 Reentrant origami-based metamaterials with negative poisson's ratio and bistability. *Phys. Rev. Lett.* **114**, 185502. (doi:10.1103/PhysRevLett.114.185502)
16. Hanna BH, Lund JM, Lang RJ, Magleby SP, Howell LL. 2014 Waterbomb base: a symmetric single-vertex bistable origami mechanism. *Smart Mater. Struct.* **23**, 094009. (doi:10.1088/0964-1726/23/9/094009)
17. Jianguo C, Xiaowei D, Ya Z, Jian F, Yongming T. 2015 Bistable behavior of the cylindrical origami structure with kresling pattern. *J. Mech. Des.* **137**, 061406. (doi:10.1115/1.4030158)
18. Miyashita S, Guitron S, Ludersdorfer M, Sung CR, Rus D. 2015 An untethered miniature origami robot that self-folds, walks, swims, and degrades. In *2015 IEEE international conference on robotics and automation (ICRA)*, pp. 1490–1496. IEEE. (doi:10.1109/ICRA.2015.7139386)
19. Overvelde JTB, Weaver JC, Hoberman C, Bertoldi K. 2017 Rational design of reconfigurable prismatic architected materials. *Nature* **541**, 347–352. (doi:10.1038/nature20824)
20. Yasuda H, Buskohl PR, Gillman A, Murphey TD, Stepney S, Vaia RA, Raney JR. 2021 Mechanical computing. *Nature* **598**, 39–48. (doi:10.1038/s41586-021-03623-y)

21. Sitti M. 2021 Physical intelligence as a new paradigm. *Extreme Mech. Lett.* **46**, 101340. (doi:.org/10.1016/j.eml.2021.101340)
22. Nakajima K, Hauser H, Li T, Pfeifer R. 2015 Information processing via physical soft body. *Sci. Rep.* **5**, 10487. (doi:10.1038/srep10487)
23. Raney JR, Nadkarni N, Daraio C, Kochmann DM, Lewis JA, Bertoldi K. 2016 Stable propagation of mechanical signals in soft media using stored elastic energy. *Proc. Natl Acad. Sci. USA* **113**, 9722–9727. (doi:10.1073/pnas.1604838113)
24. Bilal OR, Foehr A, Daraio C. 2017 Bistable metamaterial for switching and cascading elastic vibrations. *Proc. Natl Acad. Sci. USA* **114**, 4603–4606. (doi:10.1073/pnas.1618314114)
25. Shan S, Kang SH, Raney JR, Wang P, Fang L, Candido F, Lewis JA, Bertoldi K. 2015 Multistable architected materials for trapping elastic strain energy. *Adv. Mater. Weinheim* **27**, 4296–4301. (doi:10.1002/adma.201501708)
26. Ion A, Wall L, Kovacs R, Baudisch P. 2017 Digital Mechanical Metamaterials. In *Proc. of the 2017 CHI Conf. on Human Factors in Computing Systems*, Denver Colorado USA, pp. 977–988. New York, NY. (doi:10.1145/3025453.3025624). https://dl.acm.org/doi/proceedings/10.1145/3025453.
27. Jiang Y, Korpas LM, Raney JR. 2019 Bifurcation-based embodied logic and autonomous actuation. *Nat. Commun.* **10**, 128. (doi:10.1038/s41467-018-08055-3)
28. Song Y, Panas RM, Chizari S, Shaw LA, Jackson JA, Hopkins JB, Pascall AJ. 2019 Additively manufacturable micro-mechanical logic gates. *Nat. Commun.* **10**, 882. (doi:10.1038/s41467-019-08678-0)
29. Treml B, Gillman A, Buskohl P, Vaia R. 2018 Origami mechanologic. *Proc. Natl Acad. Sci. USA* **115**, 6916–6921. (doi:10.1073/pnas.1805122115)
30. Yasuda H, Korpas LM, Raney JR. 2020 Transition waves and formation of domain walls in multistable mechanical metamaterials. *Phys. Rev. Appl.* **13**, 054067. (doi:10.1103/PhysRevApplied.13.054067)
31. Chen T, Pauly M, Reis PM. 2021 A reprogrammable mechanical metamaterial with stable memory. *Nature* **589**, 386–390. (doi:10.1038/s41586-020-03123-5)
32. Kwakernaak LJ, van Hecke M. 2023 Counting and sequential information processing in mechanical metamaterials. *Phys. Rev. Lett.* **130**, 268204. (doi:10.1103/PhysRevLett.130.268204)
33. Mei T, Chen CQ. 2023 In-memory mechanical computing. *Nat. Commun.* **14**, 5204. (doi:10.1038/s41467-023-40989-1)
34. Meng Z, Yan H, Liu M, Qin W, Genin GM, Chen CQ. 2023 Encoding and storage of information in mechanical metamaterials. *Adv. Sci.* **10**, 2301581. (doi:10.1002/advs.202301581)
35. Lee YJ *et al.* 2019 Auxetic elastomers: mechanically programmable meta-elastomers with an unusual poisson's ratio overcome the gauge limit of a capacitive type strain sensor. *Extreme Mech. Lett.* **31**, 100516. (doi:10.1016/j.eml.2019.100516)
36. Meng K *et al.* 2022 Kirigami-inspired pressure sensors for wearable dynamic cardiovascular monitoring. *Adv. Mater.* **34**, e2202478. (doi:10.1002/adma.202202478)
37. Li Y, Luo S, Yang MC, Liang R, Zeng C. 2016 Poisson ratio and piezoresistive sensing: a new route to high‐performance 3D flexible and stretchable sensors of multimodal sensing capability. *Adv. Funct. Mater.* **26**, 2900–2908. (doi:10.1002/adfm.201505070)
38. Huang X *et al.* 2022 Flexible mechanical metamaterials enabled electronic skin for real‐time detection of unstable grasping in robotic manipulation. *Adv. Funct. Mater.* **32**, 2109109. (doi:10.1002/adfm.202109109)
39. Grima JN, Evans KE. 2000 Auxetic behavior from rotating squares. *J. Mater. Sci. Lett.* **19**, 1563–1565. (doi:10.1023/A:1006781224002)
40. Grima JN, Caruana-Gauci R, Dudek MR, Wojciechowski KW, Gatt R. 2013 Smart metamaterials with tunable auxetic and other properties. *Smart Mater. Struct.* **22**, 084016. (doi:10.1088/0964-1726/22/8/084016)
41. Deng B, Raney JR, Tournat V, Bertoldi K. 2017 Elastic vector solitons in soft architected materials. *Phys. Rev. Lett.* **118**, 204102. (doi:10.1103/PhysRevLett.118.204102)
42. Coulais C, Kettenis C, van Hecke M. 2018 A characteristic length scale causes anomalous size effects and boundary programmability in mechanical metamaterials. *Nat. Phys.* **14**, 40–44. (doi:10.1038/nphys4269)

43. Jiao W, Shu H, Tournat V, Yasuda H, Raney JR. 2024 Phase transitions in 2D multistable mechanical metamaterials via collisions of soliton-like pulses. *Nat. Commun.* **15**, 333. (doi:10.1038/s41467-023-44293-w)
44. Yasuda H, Shu H, Jiao W, Tournat V, Raney JR. 2023 Nucleation of transition waves via collisions of elastic vector solitons. *Appl. Phys. Lett.* **123**, 051701. 10.1063/5.0156023. (doi:10.1063/5.0156023)
45. Herbert KM, Fowler HE, McCracken JM, Schlafmann KR, Koch JA, White TJ. 2022 Synthesis and alignment of liquid crystalline elastomers. *Nat. Rev. Mater.* **7**, 23–38. (doi:10.1038/s41578-021-00359-z)
46. Ikeda T, Mamiya J ichi, Yu Y. 2007 Photomechanics of liquid-crystalline elastomers and other polymers. *Angew. Chem. Int. Ed. Engl.* **46**, 506–528. (doi:10.1002/anie.200602372)
47. He Q, Yin R, Hua Y, Jiao W, Mo C, Shu H, Raney JR. 2023 A modular strategy for distributed, embodied control of electronics-free soft robots. *Sci. Adv.* **9**, eade9247. (doi:10.1126/sciadv.ade9247)
48. Jiao W, Shu H, He Q, Raney J. 2024 Data from: Mechanical proprioception in autonomously-reconfigurable multistable kirigami. Figshare. (doi:10.6084/m9.figshare.c.7461942)